Principles of Imaging by Nuclear Magnetic Resonance

Jason A. Koutcher and C. Tyler Burt

Dana Farber Cancer Institute and Massachusetts General Hospital, and Harvard Medical School, Boston, Massachusetts

Imaging by nuclear magnetic resonance (NMR) is a new modality for obtaining anatomic data. Magnetic field gradients are used to obtain spatial information. The advantages of NMR imaging include the ability to obtain images in multiple orientations (coronal, sagittal, and transverse), absence of ionizing radiation, and the potential to obtain chemical information. NMR images of the central nervous system have been equal to those of TCT, and in some cases superior. The utility of NMR imaging is yet to be determined, although preliminary findings are encouraging.

J Nucl Med 25: 371–382, 1984

Nuclear magnetic resonance (NMR) offers a new imaging modality that is rapidly gaining prominence in the medical literature. Initially, the medical community showed little interest in this technique, despite exhortations on its vast potential (*1*). This changed in the early 1980s, when high-quality images first became accessible. Subsequently, interest in NMR imaging has increased rapidly.

This paper will focus primarily on proton NMR imaging. Unlike a previous paper of this series (*2*), the data presented here will concentrate on methods of obtaining spatial and anatomic information.

As with many other inventions, several groups became interested in the feasibility of NMR imaging concurrently. A great impetus for NMR imaging was provided by Damadian's results (*3*) showing that normal and malignant tissue have different relaxation times. He suggested that NMR would be useful for tumor detection. Shortly thereafter, Lauterbur (*4*) published two-dimensional NMR images using a reconstruction algorithm similar to that used in transmission computerized tomographic (TCT) reconstruction. Several other techniques (*5–8*) were developed by many independent groups, and within 4 yr Damadian was able to produce an NMR image across a patient's chest (*9,10*). Over the next 5 yr, significant improvements in the quality of NMR images occurred, and it now approaches that attained by TCT.

For reprints contact: Jason Koutcher, MD, PhD, NMR Office, Research 501, Massachusetts General Hospital, Boston, MA 02114.

Research in investigating the proper use for NMR imaging (i.e., whether it will replace or supplement other modalities) is ongoing. At present, other than in the central nervous system (CNS), the relative utility of NMR imaging is yet to be determined, although preliminary data are encouraging.

Before the development of NMR systems for body scanning, much effort was expended in investigating NMR characteristics of excised tissue, particularly in comparing normal and malignant tissue. In several organ systems it was shown that by combining T_1 and T_2 it was possible to discriminate between normal and malignant tissue (*11–16*). Discrimination between benign and malignant disease was demonstrated in several instances (*14–16*).

THEORY OF NMR IMAGING

In conventional diagnostic radiology using x-rays, the data obtained are dependent solely on the attenuation of the x-ray beam by the substance in its path. Since the pictures depend on only one parameter, a knowledge of local anatomy is sufficient for interpretation of the data obtained. NMR imaging is far more complex in its physical origins, since the signal depends on multiple physical parameters.

All NMR studies use two magnetic fields (H_o and H_1) as discussed previously (*17*). Unlike NMR spectroscopy, which provides chemical information and requires a highly uniform H_o, NMR imaging provides anatomic information with a less stringent homogeneity requirement for H_o. In NMR imaging, a third magnetic

field—usually in the form of multiple magnetic gradients along the x, y, and z axes—is required. These magnetic fields will translate NMR signals at different frequencies into spatial information. In the following discussion, the z axis will be associated with the longitudinal (craniocaudal) axis of the body, while the x and y axes will comprise the right-to-left and front-to-back directions.

A linear magnetic field gradient can be generated by opposing two current loops with current flowing in the opposite directions (Fig. 1). Each current loop will generate a magnetic field perpendicular to the loop, which decreases with distance from the loop. The net field generated by the two equal but oppositely flowing currents will be a linear field gradient that cancels completely at a point midway between the coils. Therefore, the net magnetic field at the center will be only H_0 (the external magnetic field.

Since Lauterbur's first image in 1973, many techniques of obtaining spatial information by NMR have appeared. They can be divided into those that obtain images of single points (*7,18,19*), a line (*20,21*), a plane (two-dimensional images) (*4,8,22*), several planes concurrently (*23*), or an entire three-dimensional volume (*24*). Point-scanning methods have the disadvantage of being relatively slow, whereas multiplanar techniques are relatively rapid since one can obtain data from several planes in the time required to image a single plane.

TWO-DIMENSIONAL IMAGING—PLANE SELECTION

Two techniques commonly used to select a two-dimensional plane from a three-dimensional object of interest include selective irradiation and oscillating gradients. Both techniques use a linear magnetic field gradient perpendicular to the two-dimensional section to be imaged—for example, if one wanted to portray a two-dimensional slice across the abdomen, the gradient would be applied along the length of the body (Fig. 2). They differ in that one approach uses a static gradient (time independent) and the other uses a time-varying gradient.

The selective-irradiation technique (*25*) uses a linear magnetic field gradient that does not vary with time during the radio frequency (rf) pulse. As stated above, one can design the field gradients so that at the center of the gradient there will be no contribution (net magnetic field = H_0), whereas there will be a negative field contribution on one side of the center (net field $<H_0$) and a positive contribution on the other side (Fig. 1). If we let G_z represent the linear field gradient along the axis z, the net field, $H = H_0 + G_z$, will therefore increase linearly along the length of the object. By using a narrow-frequency rf pulse, specifically designed to excite nuclei only within a small range of frequencies, one can select a plane in which the nuclei will be in resonance (i.e., $\omega = \gamma(H_0 + G_z)$. In all other planes there will be a slightly different value of H, so the resonance condition will not be met. The thickness of the slice, ΔZ, can be altered by changing the strength of the gradients or the bandwidth of the rf pulse (Fig. 2). Similarly, the plane of interest can be moved by changing the frequency of radiation (a different ω will require a different H to be in resonance, resulting in a different slice), or by electronically shifting the gradient.

A second method of slice selection is the oscillating-field technique (*26*). This method is similar in that a magnetic field gradient selects a plane, but with this technique the gradient is periodically reversed during excitation (i.e., the gradient is time-dependent). There is only one plane in which the magnetic field does not vary with time (i.e., at the center, Fig. 3) and where signal will be accumulated. In any other plane, the signal obtained at any time will be blurred by the oscillating magnetic field gradient.

The z gradient is utilized in both of the above techniques to choose a plane of interest in the subject's body. The x and y gradients are not used in plane selection, but are used both separately and in combination to obtain spatial information within the selected "slice."

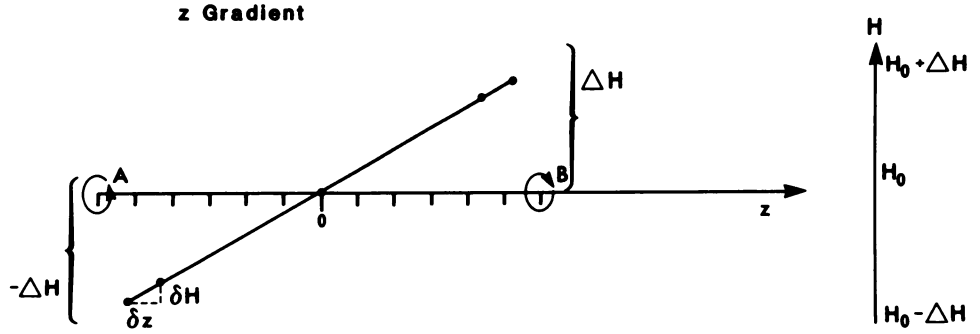

FIG. 1. Linear magnetic-field gradient is generated by 2 current loops (A and B) with current flowing in opposite directions. Each loop generates a magnetic field directed along z but directions are opposed. They therefore cancel completely at midpoint (0), leaving only main H_0 field. At position of loop A, field will be minimum ($H_0 - \Delta H$), while it will be at maximum ($H_0 + \Delta H$) at loop B. There is constant linear increase in field (δH) with distance (δz). Spatial information is based on direct correspondence between H and position (z).

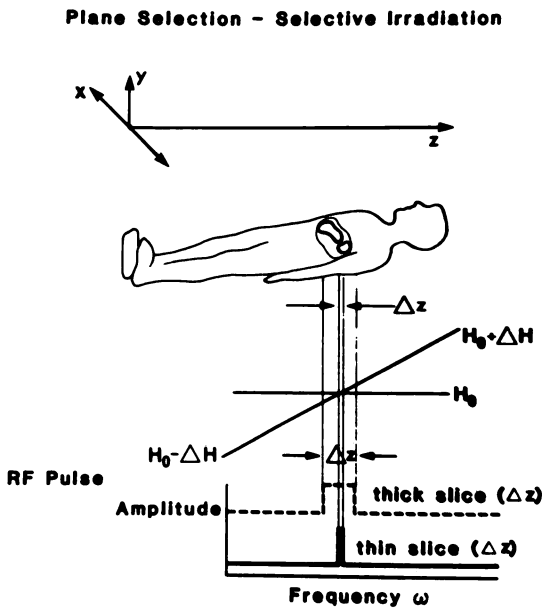

FIG. 2. Linear gradient is imposed along length of the body (z axis). Appropriate cross-sectional image is selected by frequency of radiation (ω), since resonance will be obtained only where ω and H (magnetic field) satisfy Larmor equation. Thickness of plane, Δz, depends on whether broad-band (thick slice) or narrow-band (thin slice) rf pulse is used. Plane selected can be changed by using different frequency of radiation or by moving patient.

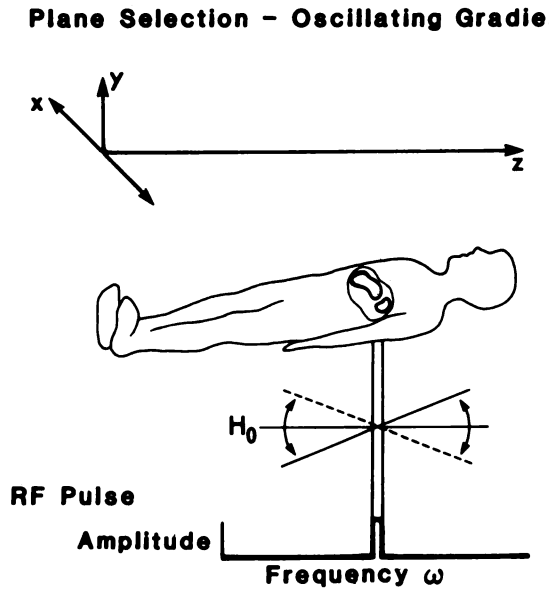

FIG. 3. Cross-sectional (xy) plane is chosen by using time-dependent z gradient. Gradients are periodically reversed so signal accumulated at any point (except midpoint) will be negated when gradient is reversed.

Both the x and y gradients can be used separately to produce gradients along their respective axes. However, they can also be combined at differing gradient strengths to form a single unified magnetic gradient at any angle in the xy plane. This resultant variable-angle gradient is essential for the projection reconstruction technique discussed below.

PLANAR IMAGING

Several techniques exist to obtain spatial information from a two-dimensional (planar) object. A commonly used method is reconstruction from projections (*4*), which will probably be familiar to the reader since it is the same technique used in TCT reconstruction.

Consider a sample containing two cylinders of water, viewed from above, as shown in Fig. 4. By exposing the sample to the appropriate radiofrequency, one can obtain a free induction decay (FID) that, after Fourier transformation, would be a single peak as in Fig. 5. However, imposing a magnetic gradient along one direction (y) of the sample would lead to a range of possible resonance frequencies, ω_i (i = A,B,C, etc.), each one satisfying the Larmor equation ($\omega_i = \gamma H_i$; i = a,b,c, etc.) at a different point along the y axis (since H increases linearly along the y axis).

Hypothetically, one could use an infinitely sharp spectral frequency, ω_A, which has a corresponding resonance field H_A to obtain a spectrum (Fig. 4) consisting of only one peak (at H_A where the Larmor equation is satisfied). Switching to a slightly higher frequency, ω_B, (again using a very sharp spectral frequency), which has a corresponding resonance field, H_B, would lead to a spectrum with a single peak but at a slightly higher magnetic field, corresponding to a point farther along the y-axis. The intensity of this peak would be greater than that of the first peak, since it would intercept a larger part of the small cylinder. Signal would arise from a single location along the y-axis, but with no spatial restriction along x.

Similarly, one could repeat the experiment many times, successively incrementing the spectral frequency (while maintaining a narrow bandwidth) and thus obtaining spectra with peaks corresponding to all the locations of the water. This is shown in Fig. 4B; Fig. 4C demonstrates the effect of combining all the peaks onto one plot to obtain a "spectrum" for display purposes. Alternatively, the entire set of experiments could be done simultaneously with one broader rf pulse that would encompass all the necessary frequencies. The result of this would be a spectrum tracing the envelope of the peaks, or a "smoothed version" of the numerous spectral peaks. This would give a partial outline of the two original circles in the plane (Fig. 4D).

In this experiment, spatial information in one dimension is defined by the magnetic field (because the gradient increases linearly across the object). The magnetic field and the frequency spectra are also linearly related through the equation $\omega = \gamma H$. The frequency spectra can therefore be used to make a spatial plot of the water content of the sample. The spectrum at the bottom of Fig. 4 represents a one-dimensional projection

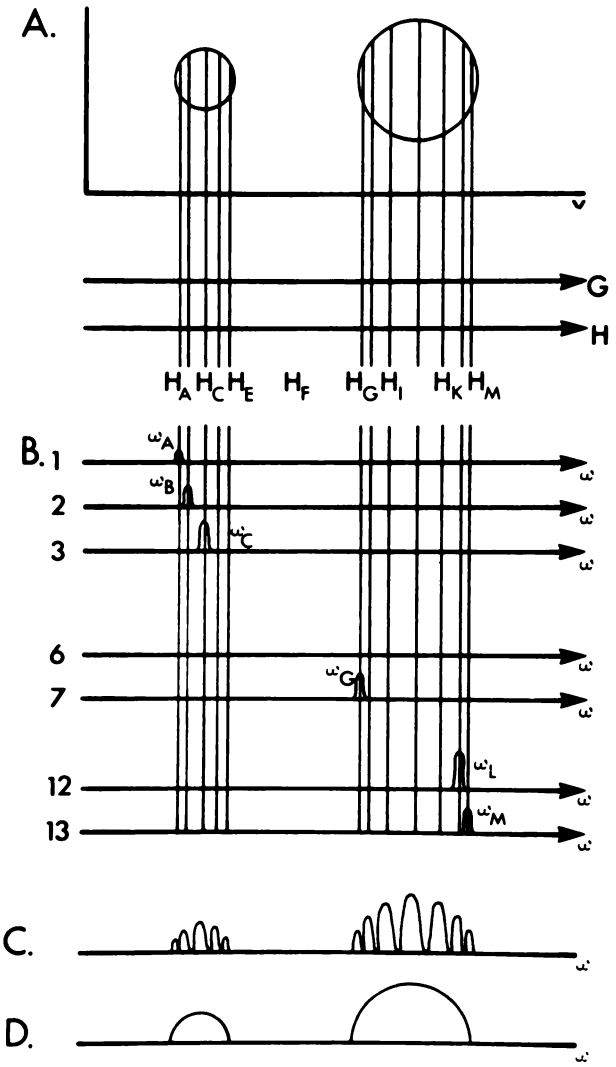

FIG. 4. A: Linear gradient G is imposed along y direction, with uniform field H_0 present. Sample consists of two cylinders of water, seen in cross section. B: Using very sharp radiofrequency pulse ω_A (which has corresponding resonance field H_A), only single peak is seen at position corresponding to H_A. Using slightly higher (but very sharp) frequency, ω_B, peak is seen only at position corresponding to H_B (not labeled), since that is only position at which resonance equation is satisfied. Using frequency ω_c (with corresponding resonance field H_c), signal is seen only at H_c. Signal strength is stronger because spatial position corresponding to H_c would intercept larger part of circle. Similarly, for successive rf pulses. Note that at field corresponding to H_F there would be no signal, since there is no water there. C: If one plotted all successive peaks on one axis, there would be series of peaks whose envelope would approximate half of outline of cylinders. D: Alternatively, if one used single broader radiofrequency pulse, encompassing all of resonant frequencies ($\omega_A \rightarrow \omega_M$) one would obtain half of outline of cylinders in single experiment.

of the image. This localizes the signal in one dimension; i.e., along the y-axis, but without defining its location along the x-axis. Figure 6 shows that if one takes projections with the magnetic gradient at different angles, different spectra will appear. This is because the object has been defined in only one dimension and would appear differently, viewed from a different angle. By obtaining multiple spectra or projections with the magnetic gradient at various angles, a two-dimensional image can be constructed in a manner analogous to x-ray TCT (Fig. 6).

A commonly used alternative method of obtaining a two-dimensional image is called Fourier zeugmatography (*8*). The technique requires gradients in both dimensions of the plane (G_x is the gradient in the x direction and G_y is the gradient in the y direction). The first gradient G_x is turned on for a short period and after it is off, G_y is applied, an FID is collected, and the signal is Fourier-transformed. The initial gradient (G_x) is a "phase-encoding gradient," whereas G_y is a "frequency-encoding" gradient.

Phase encoding is generated by the magnetic field gradient G_x, which will generate different magnetic field strengths at different locations along x. The nuclei exposed to the higher magnetic fields will precess faster. (The precession frequency ω is given by the Larmor equation $\omega = \gamma H$.) At higher values of H along x, ω will also be higher (i.e., the nuclei will precess faster). When G_x is removed, all the nuclei will again precess at the same frequency but the previous difference in precession frequencies will be evident by a difference in the phase angle (see the section on T_2 in Ref. *17* for a brief discussion of phase). The second gradient, G_y, is used in a manner similar to the gradients in projection reconstruction, i.e., frequency encoding, as discussed previously. The value of the magnetization at any point in the plane can be characterized by knowing both the frequency and the phase angle.

Many repetitions of the cycle using increasing values of G_x are necessary to obtain a complete data set fully characterizing the phase angle. The number of different gradient values required is equal to the number of volume elements (voxels) desired. The corresponding points of each of the projections generated by the different G_x

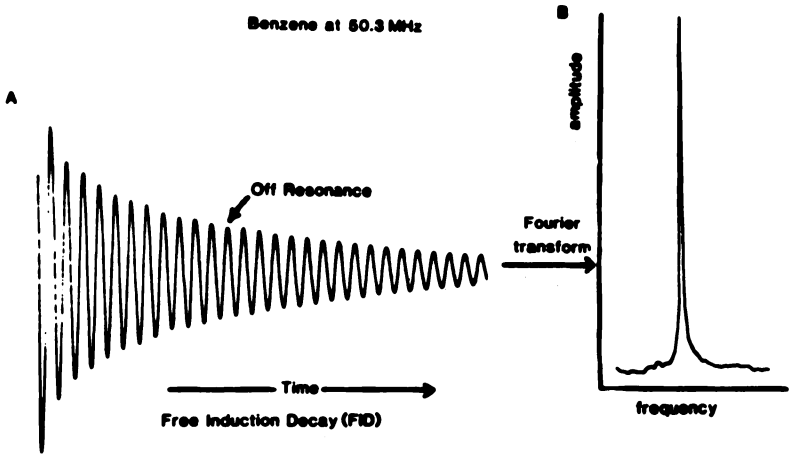

FIG. 5. A: Off-resonance Free Induction Decay (FID) of benzene (C-13), showing decaying sine wave of single frequency. Similar FID would be expected from H_2O. B: After Fourier transformation, signal is transformed into spectrum with single narrow peak.

gradients undergo a second Fourier transformation to obtain an image (Fig. 7).

It would be useful at this point to summarize the foregoing discussion. The imaging techniques discussed use multiple magnetic gradients. Referring back to Figs. 2 and 3, one can initially choose a plane of imaging by using a linear gradient along z (either by selective excitation or oscillating gradients). The selective-excitation technique requires a narrow rf bandwidth (sharp spectral frequency) to select the plane of interest, whereas the oscillating-gradient method uses broad band radiation radio frequency. One can then image the plane selected by using gradients in the x and y direction (by techniques such as projection reconstruction or Fourier zeugmatography). These also require a narrow rf pulse (although not as sharp as the hypothetical single-frequency rf pulse discussed above).

After using a method of plane selection and then reconstructing the two-dimensional image, a different plane can be chosen, and so on until a whole series of planar images are acquired, thereby obtaining three-dimensional data. (With the multiplanar technique, several planes can be imaged simultaneously.) Alternatively, one can use a true three-dimensional technique to image an object. One would then obtain data from the whole object and then reconstruct pictures of any two-dimensional sections desired. The three-dimensional techniques are basically extensions of the methods used in two-dimensional imaging, and since they do not differ significantly from a conceptual point of view, they will not be discussed here.

CONTRAST AND PULSE SEQUENCES

One of the key differences between NMR and TCT imaging is that TCT intensities depend only on tissue attenuation of the x-ray beam, whereas NMR signal intensities depend on several parameters. These include ρ (proton spin density—to be discussed below), T_1, and T_2. There are a number of pulse sequences that can be used to accentuate these different parameters, which will lead to different tissue contrast for identical samples depending on which parameter is accentuated.

The parameter that is least useful for tissue contrast is ρ, the mobile proton spin density. In simplest terms, this parameter reflects all the protons in the sample—particularly mobile water and fat protons—that will give rise to an NMR signal. Protons in the bony matrix are not freely mobile and do not give an NMR signal.

T_1 and T_2 are the spin-lattice and spin-spin relaxation parameters, discussed previously (*17*). Adjacent organs may have differing T_1 and T_2 relaxation times, which will lead to differences in the intensity of the NMR signal

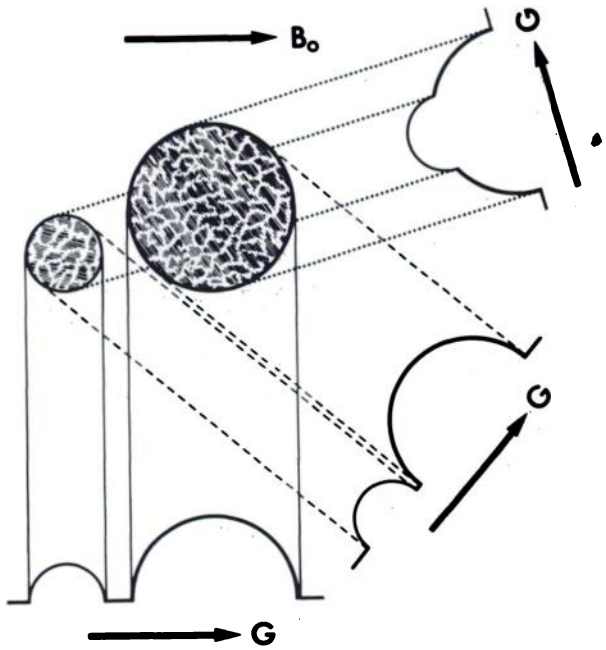

FIG. 6. Sample is "viewed" from multiple angles by varying magnetic gradient in xy plane. Gradient must be varied over at least 180°. With multiple "pictures" taken at different angles, sample projects differently. Image is reconstructed by mathematical techniques used in x-ray CT reconstruction. From Ref. *27*, with permission.

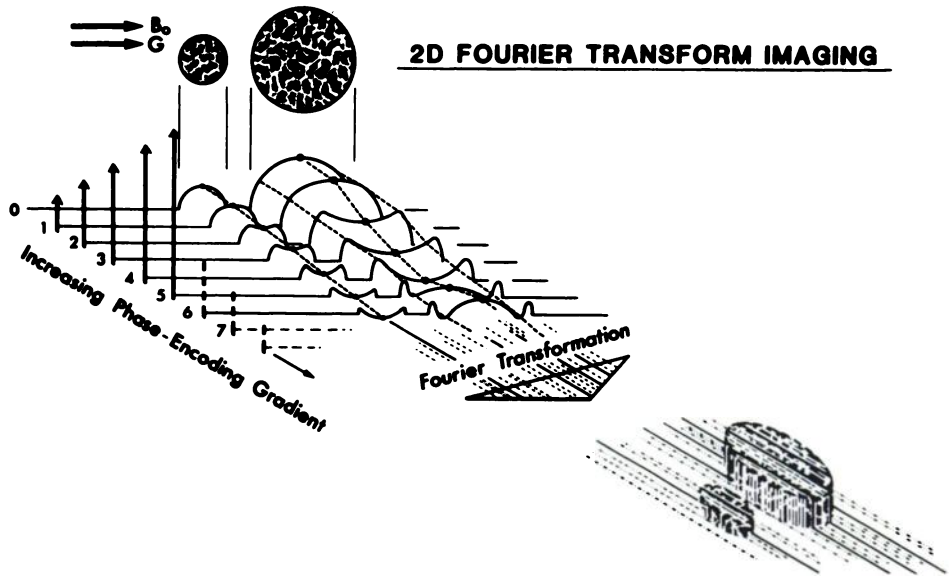

FIG. 7. Fourier zeugmatography requires use of gradients in both x and y directions. Gradient G_x is phase-encoding gradient and is at right angles to G_y gradient. Magnitude of G_x is raised sequentially from zero in small steps. NMR "spectra" become "phase distorted" by application of this second gradient. Corresponding points from each projection then undergo second Fourier transformation to generate final image. From Ref. *27*, with permission.

if a judicious choice of imaging parameters (pulse sequence and pulse interval) is made. Different T_1's and T_2's are the usual causes of image contrast between adjacent tissues in NMR.

Before discussing various pulse sequences used in NMR images, it would be useful to review briefly the concept of pulse widths and their physical interpretation. As noted in the first paper of this series, subjecting the equilibrium magnetization vector M to a radiofrequency (H_1) pulse will rotate M (the magnetization vector) from the z-axis. The angle through which it is rotated (α) depends on the H_1 field strength and the length of time the radiofrequency is on (i.e., the pulse duration). A 90° pulse rotates M from the z-axis into the xy plane, while a 180° pulse inverts M to the -z direction.

The simplest radiofrequency pulse sequence would be the repetitive use of a 90° pulse with a minimum interval $5 \times T_1$ between pulses (pulse interval). As was mentioned in the first article in the series, rotating the magnetization by 90° into the xy plane produces a maximal signal. Waiting a period of $5 \times T_1$ will allow the magnetization vector to return to equilibrium (i.e., back to its original position along the z-axis) and the next FID will be unaffected by the previous pulses, i.e., there will be no saturation (see Ref. *2* for discussion of saturation). The image intensity obtained using this type of sequence will reflect all the mobile protons in the sample, i.e., a proton spin density map. Unfortunately, this is not particularly useful since the variation of proton spin density from tissue to tissue (i.e. primarily protons in H_2O) is minimal.

A somewhat more effective technique would be to use a 90° pulse but to repeat it at a rate faster than $5 \times T_1$, [saturation recovery (SR) or partial saturation) usually at a rate approximating the average T_1 (Fig. 8). This would have the advantage of collecting data more rapidly (since one could repeat the pulse about five times as fast as before) and more importantly, there would be some effect of differential saturation between adjacent tissues. If two adjacent tissues had different T_1's, the tissue with the shorter T_1 would have returned closer to equilibrium, and therefore, when the pulse was repeated, would give a stronger signal (Fig. 9). Therefore, tumors that have longer T_1's than normal tissue (*3,11–16*) would be expected to give a lower signal intensity than adjacent tissue. The effect of different T_1's is also seen with fluid flow, which is discussed briefly later. The use of this "T_1-weighted" sequence using a short pulse interval (comparable to T_1) would lead to image contrast based on T_1 differences.

There is one other pulse sequence, which makes use of a single repetitive pulse (Fig. 8). The steady-state-free-precession (SSFP) technique consists of a train of pulses separated by an interval τ that is short relative to T_2. (In tissue, T_1 is approximately ten times T_2.) The signal intensity is a complicated function of T_1/T_2. The image intensity is therefore quite hard to interpret in terms of individual relaxation parameters.

A pulse sequence that makes use of two pulses of different length is the inversion recovery (IR) sequence shown in Fig. 10. This pulse sequence also yields T_1-weighted information. It consists of an initial 180° pulse that inverts the magnetization into the -z direction. After an interval τ, during which some relaxation of the net magnetization in the z direction occurs, a second pulse of 90° rotates the magnetization vector into the xy plane, wherein a signal can be measured. The inversion-recovery technique yields more T_1 contrast than the sat-

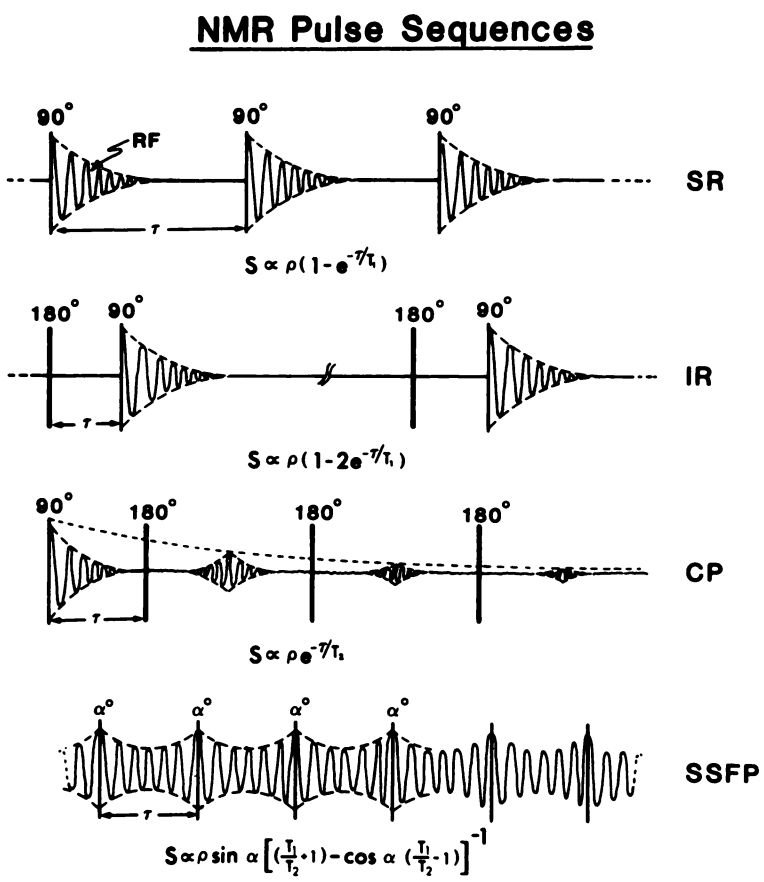

FIG. 8. Many different pulse sequences can be used in NMR imaging. In saturation-recovery (SR) and inversion-recovery (IR) sequences, signal intensities are T_1-weighted. In Carr-Purcell spin-echo sequence (C-P), signal is T_2-weighted. Steady-state-free-precession sequence (SSFP) yields image whose intensity is dependent on T_1/T_2 ratio. From Ref. *27*, with permission.

uration-recovery method. The image intensity, S, for the inversion-recovery method is given by:

$$S \propto \rho\,(1 - 2e^{-\tau/T_1})$$

T_2-weighted images can be obtained by the use of a 90°-τ-180° "spin echo" technique (*28*). As mentioned in the first paper of this series, the magnetization vector, M, is actually a sum of the individual spin magnetic moments. In an inhomogeneous field such as is used for NMR imaging, the various spins will be exposed to slightly different magnetic fields, and therefore each spin will precess at a slightly different frequency, ω.

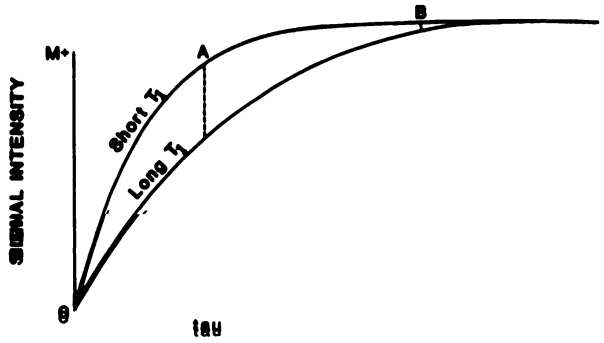

FIG. 9. Signal intensity as function of pulse interval (τ) for 2 samples with different T_1's. If one selects long value for τ, there will be no difference in signal intensity. If one chooses short τ, sample with shorter T_1 will have greater intensity, since it will be less saturated. Choice of correct pulse interval (τ) can lead to differential saturation between adjacent tissues, causing image contrast.

In a spin-echo experiment, one initially applies a 90° pulse rotating the magnetization (M) into the xy plane. After some time τ, the nuclei will no longer all be precessing at the same frequency because of the slight field inhomogeneities. The effect of this is seen in Fig. 11. The nuclear-spin moments will have a range of frequencies instead of all being aligned along y, and will appear to fan out. Application of a 180° pulse rotates each magnetic moment through the xz plane, and the individual spins will subsequently come back into phase for an instant, yielding a signal—a "spin echo." The spins will subsequently dephase again. One can use a train of 180° pulses, i.e., 90-τ-180-2τ-180-2τ-180, etc. The 180° pulses at times 3τ, 5τ, 7τ, etc., will cause the spins to refocus at 4τ, 6τ, 8τ, etc., yielding further spin echoes (*29*). The images obtained by this 90-τ-180 spin-echo technique are T_2-weighted, since the signal intensity is given by:

$$\rho e^{-\tau/T_2}$$

Alternatively, an image based on a T_1 map can be constructed. This requires using either the inversion-recovery or the saturation-recovery sequence to obtain repeat images at several values of τ (i.e., obtain multiple images with different pulse intervals). By plotting the signal intensity against τ for each point on the image, a T_1 for each point is obtained—i.e., a T_1 map. The ac-

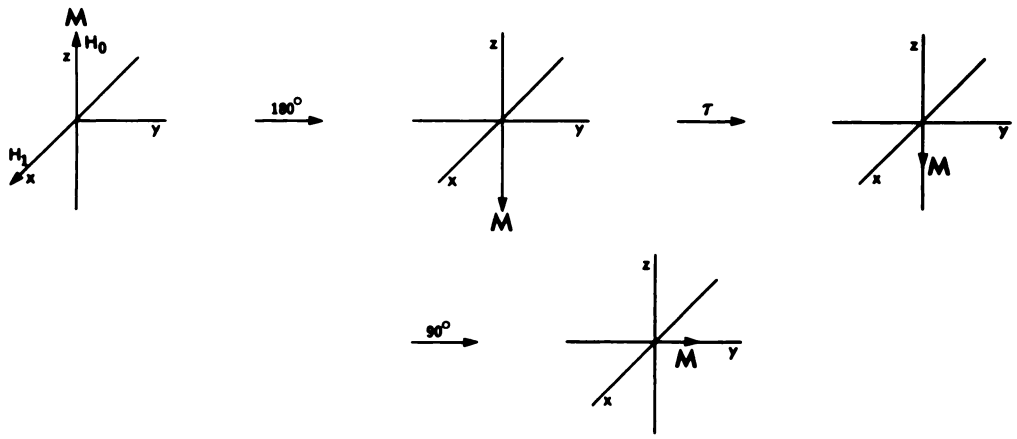

FIG. 10. Behavior of magnetization vector (M) in inversion-recovery (IR) experiment. M is initially along z-axis. After 180° H_1 pulse along x-axis, M is inverted to -z axis. After some further time τ, M is reduced because of spin-lattice relaxation. M is then rotated into xy plane by 90° pulse, and its magnitude can then be measured.

curacy of the "map" will depend on many factors, including spatial resolution (large volumes will have tissue heterogeneity, each volume element will have a distinct T_1, and if spatial resolution is poor, one will get an "averaging" effect), the number of τ values (i.e., the number of images obtained, which is analogous to the number of points for a T_1 experiment), the effect of motion or flow in the imaged volume (respiratory, cardiac, or patient movement), H_0 and H_1 homogeneity, and the accuracy of the 90° and 180° pulse durations.

Similarly, a T_2 map can be constructed using multiple 90-τ-180 pulse sequences or (in reality) by measuring successive spin echoes [which requires a modification of the spin-echo experiment developed by Meiboom and Gill (*30*)]. The accuracy of both T_1 and T_2 maps available with the present instrumentation should probably be interpreted with great caution.

The final factor that will be considered in this discussion on contrast is the effect of fluid flow. Blood flow has been studied by NMR since 1959 (*31*), but its effects on image intensity are complex. Freely flowing fluid (such as blood in the major vessels) will sometimes appear as an area of relative low signal intensity because of its elevated T_1. As mentioned previously, if the rf pulse is repeated in an interval shorter than $5 \times T_1$, the phenomenon of saturation will lead to decreased signal intensity. In T_1-weighted images (usually inversion-recovery or saturation-recovery), samples with longer T_1 will have relatively lower signal intensities than those with shorter T_1's (Fig. 9). Blood has a longer T_1 than adjacent tissue. Alternatively, in a T_2-weighted sequence, signal from blood may appear more intense because of a relatively long T_2 (Fig. 12).

Moreover, the effect of flow itself on the image is complex. Crooks et al. (*32*) have shown that the intensity of the NMR signal at different velocities is a complex function of flow velocity, tissue T_1, and pulse-sequence-timing parameters. Using a single-plane partial-saturation pulse sequence, there is signal enhancement at low flow rates, whereas at higher flow rates the signal decreases. The enhanced signal at low flow rates is caused by the introduction of "new" nonexcited protons into the imaging volume. These protons will not be saturated, as would stationary protons that have been exposed to the previous radiofrequency radiation. They are moving slowly enough, however, so that they can be "excited" and their signal measured while within the volume being imaged. At high flow rates, the nuclei will leave the volume element before signal measurement (which requires a small but finite time, depending on the pulse sequence and pulse intervals). Therefore, at high flow rates, the NMR signal will be decreased.

By this time the reader will appreciate that the effective use of an NMR instrument will require more than a simple knowledge of anatomy, for the options involved are numerous, they include different pulse sequences, different parameters that can be measured (ρ, T_1, T_2), the future possibility of imaging other nuclei (Na-23, F-19, P-31), and the possibility of using surface coils to obtain high-resolution spectra. The early clinical work has emphasized the kind of anatomical imaging familiar to the radiologist, but radiologists may well be advised to review their biochemistry. Clearly NMR technology will require the support of people trained in the physical sciences.

The significance of these multiple options was readily appreciated by Buonanno et al. (*33*). In a very early study, a patient with an astrocytoma was imaged using an inversion-recovery (IR) and a saturation-recovery (SR) sequence (both are T_1-weighted). A lesion that was not seen on TCT scan could be clearly discerned on the IR image but not on the SR. The appropriate choice of pulse sequences, pulse intervals, etc., will be crucial if NMR is to be developed to its full potential.

INSTRUMENTATION

The central component of an NMR imaging system is the magnet. While the other components [gradient

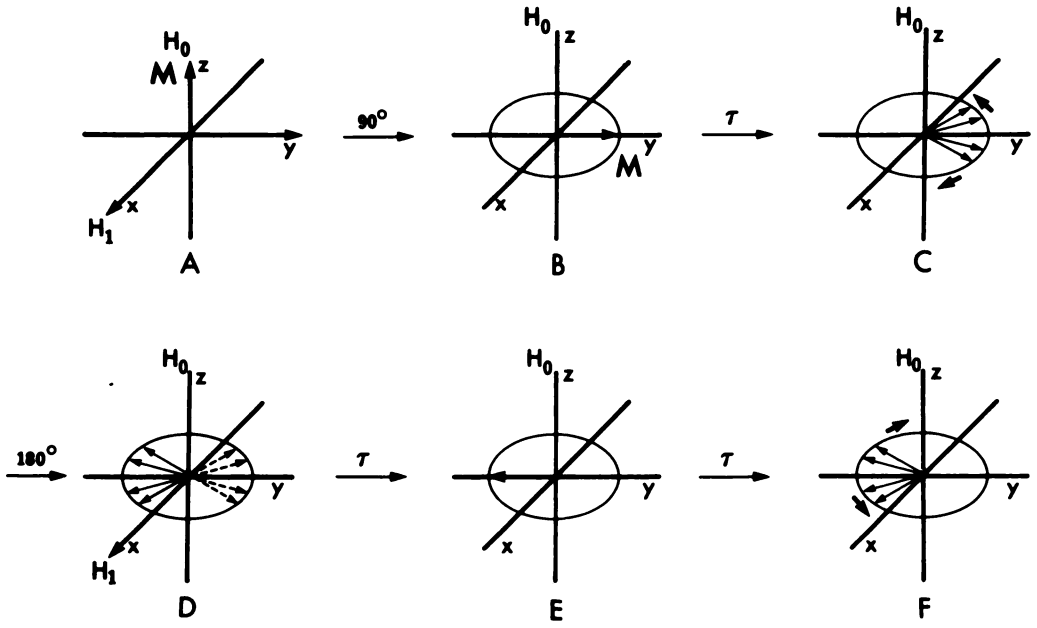

FIG. 11. Spin-Echo Experiment. (Adapted from Ref. *47*.) A: At equilibrium, magnetization (M) is along z. H_1 field is applied along x, and 90° pulse is delivered. B: 90° pulse rotates M into xy plane along y axis. C: Various nuclei will be exposed to slightly different H_0 magnetic fields. Those exposed to higher magnetic fields will rotate faster (clockwise) while those exposed to lower fields will move more slowly (counterclockwise). D: 180° pulse is applied along x, inverting nuclear spins by 180° from their previous positions (- - - →) through xz plane (→). Nuclei will continue to rotate out of phase with each other. E: Nuclei rephase along -y axis leading to observable signal, spin echo. F: Nuclei dephase again. Note that one can apply another 180° pulse to get another echo along y (not shown) and this sequence can be repeated several times and multiple "echo" signals observed (*29*).

system, rf coils, spectrometer (transmitter and receiver), power amplifier, computer] are equally important, far more attention has been paid to the magnet. This is because of the wide range of choices among magnets (permanent, resistive, or superconducting magnets, the last having the largest field range), each with its own advantages and disadvantages. For a more complete discussion of instrumentation, the reader is referred to two recent reviews (*34*,*35*). The present discussion will be limited to a brief description of the various types of magnets and their relative advantages.

Initial papers on the subject of imaging and magnetic field strength suggested that at frequencies higher than 30 MHz (7.5 kG for proton NMR), there would be problems with rf penetration in the body and energy dissipation (*36*). However, recent images suggest that, as with conventional NMR spectroscopy, higher field strengths (including magnetic fields >7.5 kG) lead to higher signal-to-noise ratios (S/N) in images. High-field images (>30 MHz) fail to demonstrate any of the theoretical difficulties expected. Comprehensive experimental evidence for an optimal maximal field strength for ^1H NMR is lacking.

In conventional NMR spectroscopy, S/N is proportional to $H_0^{7/4}$. The increase in S/N with higher magnetic fields may be only linear (*37*) in imaging studies, but the added S/N might still justify the need for higher magnetic field strengths. Another advantage to higher field strengths (noted in the first paper of this series) is that the separation between peaks due to chemical shifts increases directly with field strength. While it is premature at present to expect valuable chemical-shift data from an imaging experiment, recent findings suggest that it may be useful (*38*). The availability of higher-field magnets will be useful, from the perspective of both sensitivity and resolution if chemical-shift data are to be obtained.

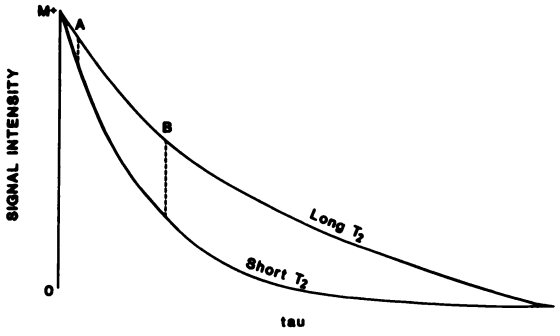

FIG. 12. Signal intensity is plotted as function of pulse interval (τ) for two samples with different T_2's. If one uses long τ there will be no difference in signal intensity. If one chooses short τ, samples with longer T_2 will have *greater* signal intensity than those with short T_2. Choice of appropriate τ value will yield different signal intensities for samples with different T_2's. Note that effect of long T_2 on signal intensity is reverse of effect of long T_1 (Fig. 9).

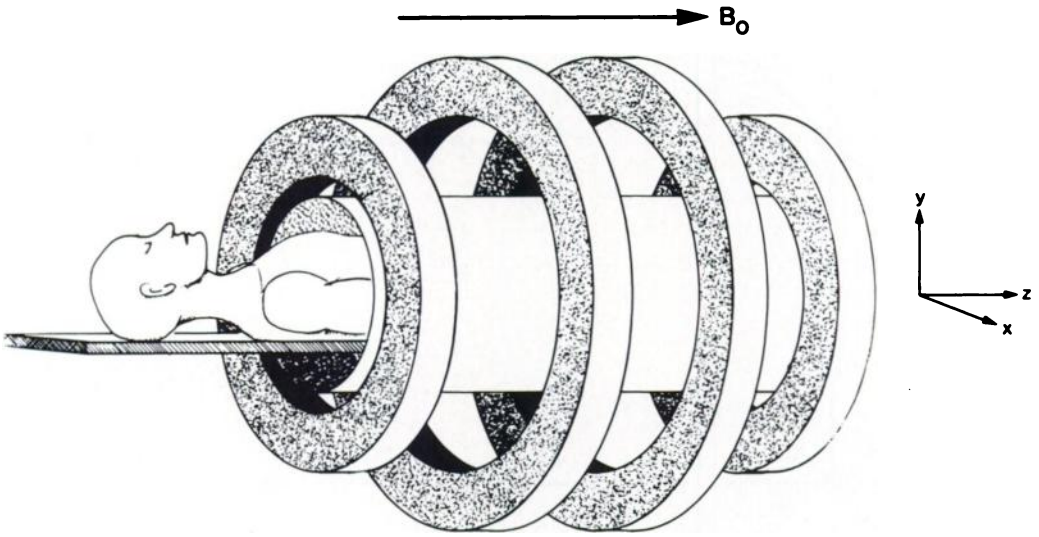

FIG. 13. Four-coil resistive magnet, similar to those used in early imaging experiments. From Ref. *39*, with permission.

Permanent magnets. Certain materials have magnetic properties that will allow construction of large permanent magnets (one is familiar with the child's horseshoe magnet). Their advantages include no energy costs (i.e., electricity or cryogenics) to operate the main field, low initial costs and minimal "fringe fields" caused by lines of force from the magnet extending outside the magnet itself. The latter may affect adjacent structures such as computers, magnetic tapes, pacemakers, etc., and can also attract ferromagnetic objects within the room. This phenomenon is sometimes referred to as "the missile effect." The disadvantages of permanent magnets include relatively low magnetic fields (3 kG) and excessive weight.

Resistive magnets. Nearly all of the initial human images were done with resistive magnets with field strengths ranging from 400 to ~1500 G. (10,000 G equals 1 tesla, so a 1500 G field is equivalent to 0.15 tesla.) A typical four-coil magnet design is shown in Fig. 13. In this magnet, direct current is passed through wires or metal tape wound around large rings, generating a magnetic field. Their field strengths are limited by the amount of current that can pass through them, which is determined by the intrinsic electrical resistance of the metal wire. They require a continuous power supply and a continuous flow of water for cooling. Their field strength (<2 kG) has been shown to be quite adequate for proton imaging, but it is unlikely that this will be sufficient for use with other nuclei. Their advantages include relatively low initial cost and easy maintenance. Their disadvantages include relatively low field strengths, the need for continuous electrical power (high electric costs), and magnetic field instabilities.

Superconducting magnets. Superconducting magnets are similar in principle to resistive magnets in that both generate magnetic fields by forcing current through an electrical coil. Superconducting magnets attain higher magnetic fields because at extremely low temperatures the intrinsic electrical resistance of the wires is zero, so that more current can be forced through them. It should be noted that one cannot drive an infinite current through superconducting wire, so the magnetic field strength should not exceed the manufacturer's specifications or the magnet will "quench" (lose field almost instantaneously). Niobium-titanium alloy is commonly used for the windings of the magnet, which is immersed in liquid helium (boiling temperature 4.2° K or −269° C) to maintain the low temperature required for superconductivity. Liquid helium is quite expensive, so much effort is expended to insulate the helium chamber as much as possible to cut down helium loss.

Care must be taken to ensure an adequate helium level so as to maintain the magnet at 4.2° K when the magnet is superconducting. If the temperature of a section of the magnet rises above the temperature of superconductivity, the magnet may go normal and "quench," leading to a rapid dissipation of a large amount of electrical energy (due to the large currents in the wire loop) in the form of heat which can damage the magnet. For this reason, a helium level indicator is obviously mandatory.

The advantages of a superconducting magnet include high field strength, magnetic-field, stability and low electrical costs. Its disadvantages include the high initial cost, maintenance costs including cryogenic liquids and specially trained technicians for handling them, and a large "fringing field." The latter will necessitate a larger space requirement. Note also that the price of a superconducting magnet can vary significantly depending on its field capabilities (i.e., a 15 kG magnet costs more than a 3.5 kG magnet).

It should be emphasized that although we have listed the high-field capability of a superconducting magnet

as an advantage, there is no evidence to date that the use of higher field strengths generates any additional clinically significant data. While it is true that S/N improves at high H_o and the images are better, there are data to suggest that differences in relaxation times between normal and abnormal tissue may be enhanced at lower field strength (*40*). Therefore the contrast-to-noise ratio may improve less rapidly, if at all, through use of higher magnetic fields.

SIGNAL TO NOISE

As was noted in the previous paper, the signal-to-noise ratio (S/N) for an NMR signal depends on coil design, the magnetogyric ratio (γ), sample volume and concentration, and magnetic field strength. We will briefly consider the last three. The use of "contrast" agents to enhance signal will be considered in the final paper of this series.

It is obvious that a sample with a higher concentration of nuclei generating signal will have a higher signal-to-noise ratio than that of a less concentrated sample. In biomedical imaging, unfortunately, this parameter can be varied only by increasing the "slice thickness," with consequent loss of resolution.

In a manner analogous to NMR spectroscopy, the larger the sample volume, the stronger the signal, since there will be more nuclei present. Therefore, in using two-dimensional imaging techniques, if one selects a "thick" slice (i.e., Δz is large, Fig. 2), the volume from which signal would be acquired when imaging the two-dimensional slice will be larger and will contain more nuclei, yielding a stronger signal. Alternatively, one can use stronger magnetic field gradients, which will yield higher anatomic resolution (a thin "slice") but lower S/N. The effect of different magnetic field strengths (H_o) has been discussed previously.

POTENTIAL HAZARDS OF NMR IMAGING

One of the most significant advantages of NMR over TCT is the lack of ionizing radiation (i.e., x-rays). The possible harmful aspects of NMR involve the large static field (H_o), the radiofrequency field (H_1) and rapidly switching magnetic gradient fields. Studies on both human and nonhuman cell cultures and bacteria fail to show any harmful side effects (*41–43*). Also, many researchers who have had hours of exposure have failed to note any ill effects from NMR. While further study is necessary, there is no evidence at present for any harmful effects of NMR. A review of the subject has been published (*44*).

Some of the potential areas of concern with regard to side effects involve "foreign objects" in the body: pacemakers, prostheses, surgical clips, and metal implants, etc. Preliminary studies investigating the effects of NMR on these "foreign objects" have appeared (*45*).

Davis et al. have studied the heating effects of surgical clips and prostheses (*46*). They suggested that surgical clips did not cause significant heat absorption, although two hip prostheses in saline did manifest significant temperature increases.

New et al. studied a variety of surgical clips. They found that sufficient torque was exerted on five aneurysm clips to suggest that patients will be at risk for clip dislocation and hemorrhage (*45*). Clips of 10–14% nickel were found to be relatively safe. Dental amalgam did not produce image distortion, but stainless steel in dentures and braces did.

SUMMARY

The physical basis of proton NMR imaging has been presented in a qualitative manner. Techniques to select a two-dimensional plane from a three-dimensional object were presented. The principles behind some of the two-dimensional imaging techniques were discussed. True three-dimensional NMR imaging represents an extension of the two-dimensional process. The complexity of NMR imaging was demonstrated by the several pulse sequences available, and other variables (pulse intervals and use of other nuclei) were noted. The advantages and disadvantages of the various types of magnets (primarily cost and "fringe field") were also considered. At present, NMR biomedical imaging is limited to protons but eventually other nuclei (F-19, P-31, Na-23) may be imaged.

ACKNOWLEDGMENTS

The authors thank Edith Bell and Marlene Gillis for secretarial assistance and DeeDee Correia for administrative help.

REFERENCES

1. DAMADIAN R: Nuclear magnetic resonance: a noninvasive approach to cancer. *Hospital Practice* 12:63–70, 1977
2. BURT CT, KOUTCHER JA: Multinuclear NMR studies of naturally occurring nuclei. *J Nucl Med* 25:237–248, 1984
3. DAMADIAN R: Tumor detection by nuclear magnetic resonance. *Science* 171:1151–1153, 1971
4. LAUTERBUR PC: Image formation by induced local interactions: examples employing NMR. *Nature* 242:190–191, 1973
5. ABE Z, TANAKA K: U.S. Patent 3,932,805, 1973
6. MANSFIELD P, GRANNELL PK: NMR "diffraction" in solids? *J Phys C: Solid State Phys* 6:L422–L426, 1973
7. HINSHAW WS: Spin mapping: the application of moving gradients to NMR. *Phys Lett* 48(A):87–88, 1974
8. KUMAR A, WELTI D, ERNST RR: NMR Fourier zeugmatography. *J Mag Res* 18:69–83, 1975
9. DAMADIAN R, GOLDSMITH M, MINKOFF L: NMR in cancer. XVI. FONAR image of the live human body. *Physiol Chem Phys* 9:97–100, 1977
10. DAMADIAN R, MINKOFF L, GOLDSMITH M, KOUTCHER JA: Field-focusing nuclear magnetic resonance (FONAR). Formation of chemical scans in man. *Naturwissenschaften* 65:250–252, 1978

11. KOUTCHER JA, GOLDSMITH M, DAMADIAN R: Nuclear magnetic resonance in cancer, X: A malignancy index to discriminate normal and cancerous tissue. *Cancer* 41:174–182, 1978
12. GOLDSMITH M, KOUTCHER JA, DAMADIAN R: NMR in cancer, XI: Application of the NMR malignancy index to human gastro-intestinal tumors. *Cancer* 41:183–191, 1978
13. GOLDSMITH M, KOUTCHER JA, DAMADIAN R: NMR in cancer. XII. Application of NMR malignancy index to human lung tumors. *Br J Cancer* 36:235–242, 1977
14. GOLDSMITH M, KOUTCHER JA, DAMADIAN R: NMR in cancer, XIII: Application of the NMR malignancy index to human mammary tumors. *Br J Cancer* 38:547–554, 1978
15. MEDINA D, HAZLEWOOD CF, CLEVELAND GG, et al: Nuclear magnetic resonance studies on human breast dysplasias and neoplasms. *J Natl Cancer Inst* 54:813–818, 1975
16. FRUCHTER RG, GOLDSMITH M, BOYCE JG, et al: Nuclear magnetic resonance properties of gynecological tissues. *Gynecol Oncol* 6:243–255, 1978
17. KOUTCHER JA, BURT CT: Principles of nuclear magnetic resonance. *J Nucl Med* 25:101–111, 1984
18. DAMADIAN L, MINKOFF M, GOLDSMITH M, et al.: Field focusing nuclear magnetic resonance (FONAR): Visualization of a tumor in a live animal. *Science* 194:1430–1432, 1976
19. HINSHAW WS: Image formation by NMR: The sensitive point method. *J Appl Phys* 47:3709–3721, 1976
20. ANDREW ER, BOTTOMLEY PA, HINSHAW WS, et al: NMR images by the multiple sensitive point method: application to larger biological systems. *Phys Med Biol* 22:971–974, 1977
21. MANSFIELD P, PYKETT IL, MORRIS PG, COUPLAND RE: Human whole body line-scan imaging by NMR. *Br J Radiol* 51:921–922, 1978
22. EDELSTEIN WA, HUTCHISON JMS, JOHNSON G, et al: Spin warp NMR imaging and applications to human whole-body imaging. *Phys Med Biol* 25:751–756, 1980
23. CROOKS L, ARAKAWA M, HOENNINGER J, et al: Nuclear magnetic resonance whole-body imager operating at 3.5 kGauss. *Radiology* 143:169–174, 1982
24. LAI CM, LAUTERBUR PC: True three-dimensional image reconstruction by nuclear magnetic resonance zeugmatography. *Phys Med Biol* 26:851–856, 1981
25. GARROWAY AN, GRANNELL PK, MANSFIELD P: Image formation in NMR by a selective irradative process. *J Phys* C7:L457–L462, 1974
26. BROOKER HR, HINSHAW WS: Thin-selection NMR imaging. *J Mag Res* 30:129–131, 1978
27. PYKETT IL, BUONANNO FS, BRADY TJ, KISTLER JP: Techniques and approaches to proton NMR imaging of the head. *Comput Radiol* 7:1–17, 1983
28. HAHN EL: Spin echoes. *Phys Rev* 80:580–594, 1950
29. CARR H, PURCELL E: Effects with diffusion or free precession in nuclear magnetic resonance. *Phys Rev* 94:630, 1954
30. MEIBOOM S, GILL D: Modified spin echo method of measuring nuclear relaxation times. *Rev Scient Instrum* 29: 688–691, 1958
31. SINGER JR: Blood flow rates by nuclear magnetic resonance measurements. *Science* 130:1652–1653, 1959
32. CROOKS LE, MILLS CM, DAVIS PL, et al: Visualization of cerebral and vascular abnormalities by NMR imaging. The effects of imaging parameters on contrast. *Radiology* 144: 843–852, 1982
33. BUONANNO FS, PYKETT IL, BRADY TJ, et al: Clinical relevance of two different nuclear magnetic resonance approaches to imaging of a low grade astrocytoma. *J Comput Assist Tomogr* 6:529–535, 1982
34. PYKETT IL: Instrumentation for nuclear magnetic resonance imaging. *Semin Nucl Med* 8:319–328, 1983
35. HOLLAND GN: Systems engineering of a whole body proton magnetic resonance imaging system. In *Nuclear Magnetic Resonance Imaging.* Partain CL, James AE, Rollo FD, eds. Philadelphia, W.B. Saunders, 1983, pp 128–151
36. BOTTOMLEY PA, ANDREW ER: RF magnetic field penetration, phase shift and power dissipation in biological tissue: Implications for NMR imaging. *Phys Med Biol* 23:630–643, 1978
37. HOULT DI, LAUTERBUR PC: The sensitivity of the zeugmatographic experiment involving human samples. *J Mag Res* 34:425–433, 1979
38. PYKETT IL, ROSEN BR: Nuclear magnetic resonance: in vivo proton chemical shift imaging. *Radiology* 149:197–201, 1983
39. PYKETT IL, NEWHOUSE JH, BUONANNO FS, et al: Principles of nuclear magnetic resonance imaging. *Radiology* 143:157–168, 1982
40. DAMADIAN R, ZANER K, HOR D, DIMAIO T: Human tumors detected by nuclear magnetic resonance. *Proc Natl Acad Sciences* 71:1471–1473, 1974
41. WOLFF S, CROOKS LE, BROWN P, et al: Tests for DNA and chromosomal damage induced by nuclear magnetic resonance imaging. *Radiology* 136:707–710, 1980
42. THOMAS A, MORRIS PG: The effects of NMR exposure on living organisms: I. A microbial assay. *Br J Radiol* 54: 615–621, 1981
43. COOKE P, MORRIS PG: The effects of NMR exposure on living organisms. II. A genetic study of human lymphocytes. *Br J Radiol* 54:622–625, 1981
44. BUDINGER TF: Nuclear magnetic resonance (NMR) in vivo studies: known thresholds for health effects. *J Comput Assist Tomogr* 5:806–811, 1981
45. NEW PFJ, ROSEN BR, BRADY TJ, et al: Potential hazards and artifacts of ferromagnetic and nonferromagnetic surgical and dental materials and devices in nuclear magnetic resonance imaging. *Radiology* 147:139–148, 1983
46. DAVIS PL, CROOKS L, ARAKAWA M: Potential hazards in NMR imaging: heating effects of changing magnetic fields and RF fields on small metallic implants. *Am J Roentgenol* 137:857–860, 1981
47. FARRAR TC, BECKER ED, eds: *Pulse and Fourier Transform NMR.* New York, Academic Press, 1971, p 23